AGU PUBLICATIONS

JGR

Journal of Geophysical Research: Atmospheres

RESEARCH ARTICLE
10.1002/2015JD024374

Key Points:
- Mesospheric Rayleigh lidar temperatures during 6 SSW periods between 1993–2004 were studied
- Midlatitude mesospheric coolings and warmings during SSWs are as strong as in polar regions
- Temperature anomalies are seen at a midlatitude site during every observed SSW period

Correspondence to:
L. Sox,
leda.sox@gmail.com

Citation:
Sox, L., V. B. Wickwar, C. S. Fish, and J. P. Herron (2016), Connection between the midlatitude mesosphere and sudden stratospheric warmings as measured by Rayleigh-scatter lidar, *J. Geophys. Res. Atmos.*, *121*, 4627–4636, doi:10.1002/2015JD024374.

Received 20 OCT 2015
Accepted 8 APR 2016
Accepted article online 11 APR 2016
Published online 11 MAY 2016

Connection between the midlatitude mesosphere and sudden stratospheric warmings as measured by Rayleigh-scatter lidar

Leda Sox[1], Vincent B. Wickwar[1], Chad S. Fish[2], and Joshua P. Herron[3]

[1]Center for Atmospheric and Space Sciences and Physics Department, Utah State University, Logan, Utah, USA, [2]Atmospheric and Space Technology Research Associates, Boulder, Colorado, USA, [3]Space Dynamics Laboratory, Utah State University, Logan, Utah, USA

Abstract While the mesospheric temperature anomalies associated with Sudden Stratospheric Warmings (SSWs) have been observed extensively in the polar regions, observations of these anomalies at midlatitudes are much more sparse. The Rayleigh-scatter lidar system, which operated at the Center for Atmospheric and Space Sciences on the campus of Utah State University (41.7°N, 111.8°W), collected a very dense set of observations, from 1993 to 2004, over a 45–90 km altitude range. This paper focuses on Rayleigh lidar temperatures derived during the six major SSW events that occurred during the 11 year period when the lidar was operating and aims to characterize the local response to these midlatitude SSW events. In order to determine the characteristics of these mesospheric temperature anomalies, comparisons were made between the temperatures from individual nights during a SSW event and a climatological temperature profile. An overall disturbance pattern was observed in the mesospheric temperatures associated with SSW events, including coolings in the upper mesosphere and warmings in the upper stratosphere and lower mesosphere, both comparable to those seen at polar latitudes.

1. Introduction

Sudden stratospheric warmings (SSWs) are major disturbances in the polar region of the winter hemisphere that are defined by changes in stratospheric temperature and circulation. They were first observed in 1952 via radiosonde [*Scherhag*, 1952; *Labitzke and van Loon*, 1999] and are characterized by a temperature increase of tens of degrees Kelvin, averaged over 60°–90° latitude at 10 hPa (roughly 32 km), and a weakening of the polar vortex that persists for the order of a week at 60° and 10 hPa level [*Charlton and Polvani*, 2007].

The term *sudden stratospheric warming*, although the accepted term, can be misleading. SSW effects on middle atmosphere temperature and circulation have lifetimes of 80 days [*Limpasuvan et al.*, 2004] and thus are not very *sudden*. Their effects have been seen throughout the entire atmospheric column [*Baldwin and Dunkerton*, 2001; *Labitzke*, 1972; *Whiteway and Carswell*, 1994; *Siskind et al.*, 2005; *Walterscheid et al.*, 2000; *de Wit et al.*, 2014; *Laskar and Pallamraju*, 2014; *Hoffmann et al.*, 2007; *Chau et al.*, 2010; *Goncharenko et al.*, 2010] and thus are not limited to just the *stratosphere*. They can also manifest as temperature decreases in other parts of the globe and atmosphere and thus are not only characterized by *warmings* [*Labitzke*, 1972; *Liu and Roble*, 2002; *Whiteway and Carswell*, 1994; *Siskind et al.*, 2005; *Walterscheid et al.*, 2000; *Quiroz,* 1977].

The mechanism for generating SSWs involves an increase in planetary wave (PW) activity in the upper troposphere and lower stratosphere, which then propagates upward in the stratosphere and then dissipates in a wave-mean flow interaction with the polar vortex [*Matsuno*, 1971]. Planetary waves, or Rossby waves, are the class of atmospheric wave that have the largest horizontal wavelengths and result from the pole-to-pole potential vorticity gradient created by the Earth's rotation [*Holton*, 2004; *Andrews et al.*, 1987]. The polar vortex is a cyclone centered on the Earth's wintertime pole and is characterized by strong eastward zonal winds. The increased PW activity leads to increased PW breaking [*McIntyre and Palmer*, 1983] in the polar stratosphere and the deposition of the PW's westward momentum in the polar vortex. This weakens the polar vortex and, in the case of major SSWs, reverses the zonal wind direction to westward.

The reversal of the stratospheric jet allows more eastward propagating gravity waves (GWs) to travel up into the mesosphere where, under normal winter conditions, westward propagating GWs dominate [*Liu and Roble*, 2002; *Yamashita et al.*, 2010; *Thurairajah et al.*, 2014; *de Wit et al.*, 2014]. The atypical wintertime GW

filtering and the resulting dominance of eastward GWs induce an equatorward circulation in the mesosphere, similar to what it is in summer, which leads to the cooling of the upper polar mesosphere.

Mesospheric coolings of tens of degrees have been observed in the polar regions for several decades [*Labitzke*, 1972; *Whiteway and Carswell*, 1994; *Walterscheid et al*., 2000; *Azeem et al*., 2005]. However, at midlatitudes there were shown to be only small deviations (less than 10 K) from normal wintertime temperatures in the mesosphere [*Angot et al*., 2012; *Chandran and Collins*, 2014; *Liu and Roble*, 2002]. Case studies have challenged this notion by reporting mesospheric coolings at midlatitude sites that have magnitudes of up to 30 K [*Hauchecorne and Chanin*, 1983; *Yuan et al*., 2012]. This study aims to further challenge the notion that the midlatitude stratosphere and mesosphere are unaffected during sudden stratospheric warmings by giving a climatological context using 11 years' worth of Rayleigh-scatter lidar temperatures from a midlatitude site.

This paper is organized as follows. In section 2 the methodology for classifying SSWs and the instrument and data descriptions of the Utah State University (USU) Rayleigh lidar system are given. Section 3 shows the results from the USU Rayleigh lidar temperature data set. Finally, sections 4 and 5 (respectively) present a discussion of and conclusions about the results presented in the paper.

2. SSWs and Rayleigh-Scatter Lidar Temperatures From 1993 to 2004

2.1. Classification of SSW Events

This study looks exclusively at major, Northern Hemisphere SSWs. We selected major SSWs using the same method as in *Charlton and Polvani* [2007]. Here we use NASA's Modern-Era Retrospective Analysis for Research and Applications (MERRA) reanalysis data set [*Rienecker et al*., 2011] to select the SSWs which meet the two defining criteria of major SSWs: (1) a large deviation from the mean of the temperatures zonally averaged from 60° to 90°N at the 10 hPa pressure level and (2) a reversal of the zonal mean winds from eastward to westward at 60°N and at the 10 hPa pressure level. Figure 1 shows the MERRA temperatures, zonal winds, and planetary wave zonal number 1 (PW1) amplitudes of the geopotential height for the six major SSWs between 1993 and 2004, during which there were observations made by the Rayleigh-scatter lidar (RSL) on the campus of USU (described in the following section of this paper). There were eight major SSW events that occurred between 1993 and 2004, and the USU RSL data set overlapped with six of them. Additionally, to make the distinction between major SSWs and final warmings, events were only selected in which the zonal winds reversed back to eastward for at least 2 weeks prior to their seasonal reversal to westward in spring. An example of this can be seen in Figure 1c during the March 2000 SSW when the zonal winds switch back to westward for 17 days before they make their seasonal reversal to eastward in early April.

2.2. 1993–2004 USU RSL Temperature Data

A RSL operated at the Atmospheric Lidar Observatory on the campus of USU (41.7°N, 111.8°W) from 1993 to 2004 [*Herron*, 2007; *Wickwar et al*., 2001]. It employed either a Spectra Physics gaussian coupled resonator (GCR-5) or GCR-6 Nd:YAG laser to transmit 18 W (600 mJ per pulse) or 24 W (800 mJ per pulse), respectively. Both lasers operated at a wavelength of 532 nm and pulse repetition rate of 30 Hz. The receiver was comprised of a 44 cm diameter Newtonian telescope that was optically coupled to an Electron Tubes 9954 series photomultiplier tube (PMT). The low-altitude signal was reduced by a mechanical chopper and by electronically gating the PMT. The lidar's raw signal profiles were recorded, using a multichannel scaler unit, with a time resolution of 2 min. In altitude, the raw signal was binned in 250 ns, or 37.5 m, intervals. However in postprocessing, a boxcar average was applied to the time-averaged signal with a 3 km window. In this study, the signal was also time averaged over the entire night, for each given night. This results in a variable number of hours in each night's average. The mean number of hours per night in each nighttime average in this study is 6.5 h. The gating of the PMT was set so that the tube would be fully on at altitudes of 38 km and higher. The upper altitude limit, for each night's average, was chosen to be where the lidar signal was 20 times its standard deviation. Several factors determine how good the signal-to-standard deviation ratio was at a given height for each observed night, including the following: length of the observation, laser power, atmospheric transmission, and neutral number density. Depending mostly on the number of hours in each night's average, the upper altitude limit would vary from 80 to 95 km but reached 90 km on most nights [*Herron*, 2007].

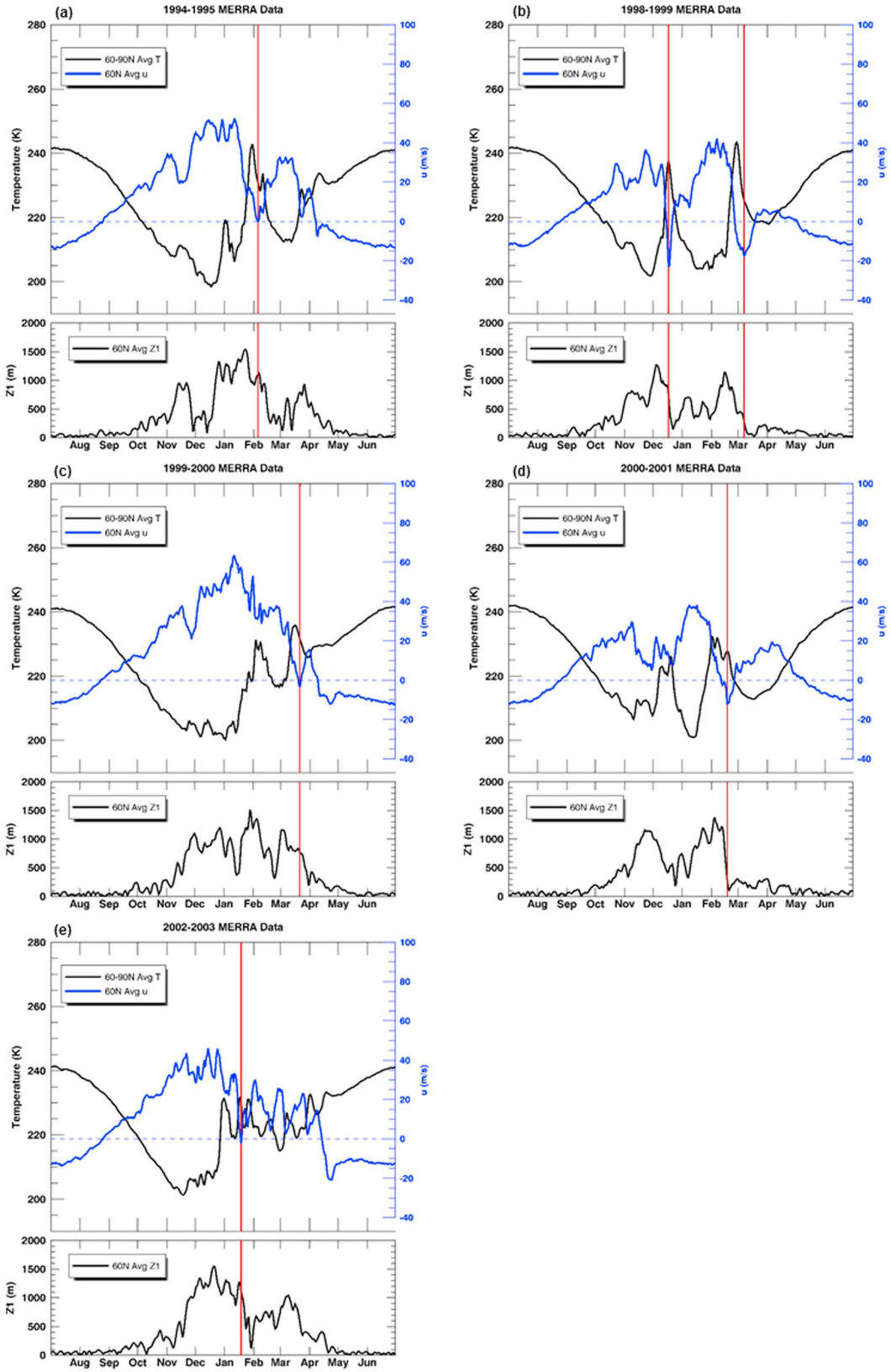

Figure 1. The 60°–90°N zonal mean temperatures (T; black curve) and 60°N zonal mean zonal winds (u; blue curve) both at 10 hPa from the MERRA database. Six SSW events between 1993 and 2004 are given (a–e). Red vertical lines mark peak dates. Note that 1998–1999 winter had two SSW events. The bottom panels of Figures 1a–1e show the PW1 amplitudes (Z1) of geopotential height zonally averaged around 60°N as a function of time.

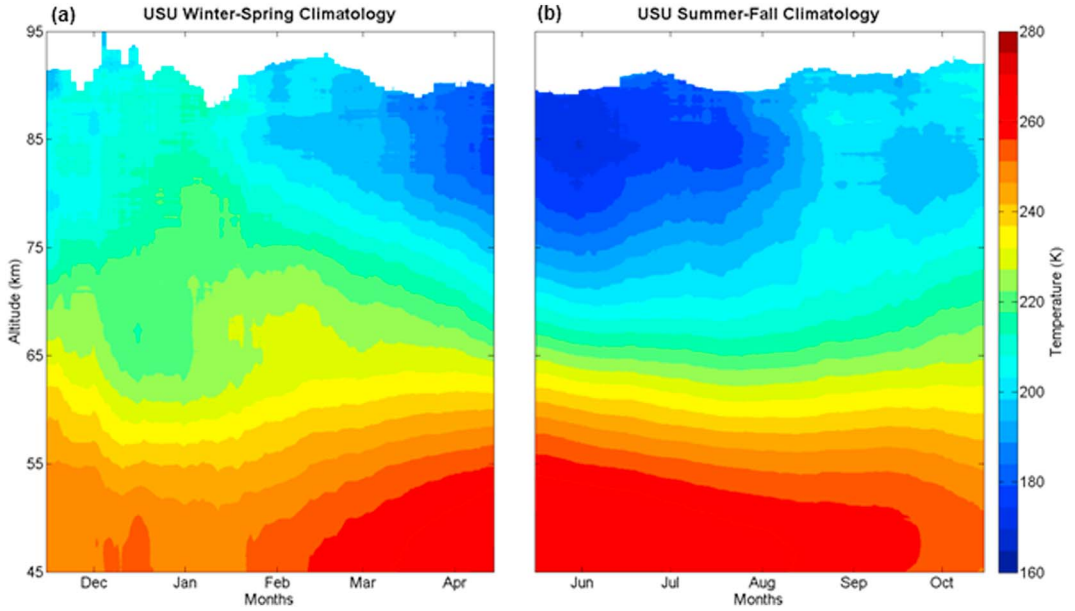

Figure 2. USU Rayleigh lidar climatology for (a) winter-spring (December-April) and (b) summer-fall (June-October) periods. The climatology was calculated using nighttime temperature measurements from 1993 to 2004.

The USU RSL data were used to calculate absolute temperatures using a modified version of the method described in *Hauchecorne and Chanin* [1980] [*Beissner*, 1997; *Herron*, 2007]. This method relies on the proportionality between lidar signal and relative density, which is then related to absolute temperature using the ideal gas law and the assumption that the measured portion of the atmosphere is in hydrostatic equilibrium. The RSL temperature integral requires a seed temperature at the highest altitude, which is used as an initial condition for the downward integration. In this study the seed temperature values were taken from the climatology of the sodium resonance lidar, formerly at Colorado State University [*She et al.*, 2000], for nights when the lidar data reached 83 km and above. For nights when the USU RSL data did not reach 83 km, a combination of the MSISE90 [*Hedin*, 1991] empirical model, and the CSU climatology was used.

The CSU temperatures were chosen as a seed temperature source due to the fact that the two lidars' data sets overlapped both temporally and in altitude and because the CSU lidar site was close in latitude and longitude (40.6°N, 105°W) to the USU lidar site. While choice of a seed temperature can introduce a systematic source of error at the upper RSL altitudes, its effect becomes exponentially smaller as one continues the temperature integration downward in altitude. If one supplies seed temperatures that are ±20 K different from the initial seed temperature at the top altitude, then by 15 km lower, the differences in the temperature curves go down to ±1 K and continue decreasing thereafter as the altitude decreases. In addition to the systematic seed temperature error, there is also a random error from photon counting that is propagated through the temperature calculation. Again, these errors decrease significantly with decreasing altitude as the signal-to-standard deviation ratio increases rapidly with decreasing altitude. For the purpose of this study, the temperatures reported above about 80 km should be conservatively considered.

A temperature climatology was calculated using over 800 nights (over 5000 h) of data collected with the USU RSL from 1993 to 2004. The climatology averaged the nighttime temperatures over a window 31 nights wide, centered on each night, and 11 years deep. Figure 2 gives the winter-to-spring (December–April) and summer-to-fall (June–October) portions of the climatology.

The climatology shows the expected seasonal change in mesospheric temperatures that range from about 170 K in the upper mesosphere to 270 K in the lower mesosphere during the summer months and then range from 205 K in the upper mesosphere to 250 K in the lower mesosphere during the winter months. Figure 3 shows example temperature profiles from the winter (3 February) and summer (4 August) portions of the climatology. The choice of 3 February and 4 August as representative climatological dates will be further

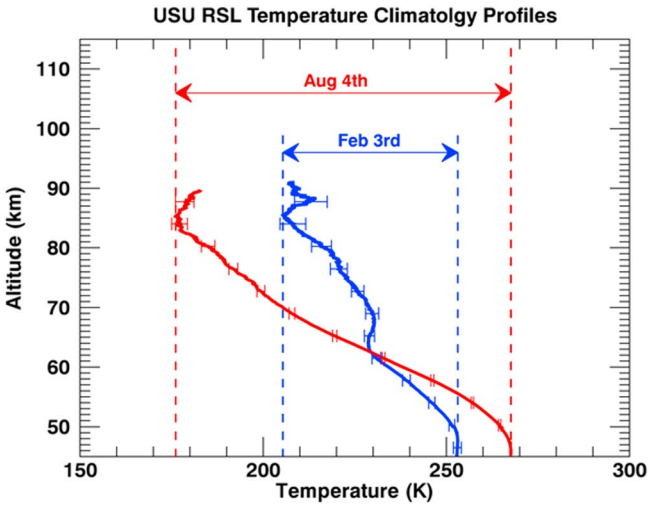

Figure 3. USU Rayleigh lidar temperature climatological profiles for a winter night (3 February, blue curve) and a summer night (4 August, red curve). The minimum and maximum of each curve defines the representative winter temperature range (205–250 K) and summer temperature range (170–270 K). Error bars shown are the RMS standard deviation of the mean for each climatological profile.

discussed in the following section. For the remainder of this paper, the winter temperature range will reference the 170–270 K range and the summer temperature range will reference the 205–250 K range.

There are also two notable cold temperature minima anomalies in the USU climatology, one occurring from about 60 to 75 km lasting from December to January and another from about 73 to 87 km lasting from mid-September to mid-October. The first minimum is likely a signature from SSWs since the RSL data overlapping with SSW events were included in the calculation of the climatology. Also, there is a corresponding warming in the upper stratosphere (45–50 km) during this same period. The second minimum is an interesting feature that has yet to be fully explained.

3. Results

There were six major SSW events that occurred between 1993 and 2004 during which there were USU RSL observations. Table 1 lists the six SSW periods along with their peak dates [*Limpasuvan et al*., 2004] or the date on which the zonal mean zonal winds were at the maximum westward value. The dates for ±40 days from the peak date are also given along with the number of nighttime RSL observations for the event period.

USU RSL temperatures for each of the six SSW event periods are shown in Figure 4. The nighttime averaged RSL temperatures were smoothed with a window of 5 days to emphasize the temporal structure. Peak dates for each event are denoted by a red vertical line. The color bars for each of the plots in Figure 4 have the same scale as the climatology in Figure 2. In all of the plots, Figures 4a–4f, the temperatures switch from the climatology's winter temperature range to its summer temperature range (Figure 3) during the SSW. This results in a warming of the upper stratosphere and lower mesosphere (45–65 km) and a cooling of the upper mesosphere (65–90 km). For the January–April 1999 (Figure 4c) and January–February 2003 (Figure 4f) events, this switch from winter-to-summer conditions happens prior to the peak date. For the November 1998 to January 1999 (Figure 4b) and January–March 2001 (Figure 4e) events, this switch happens after the peak date. The December 1994 to March 1995 (Figure 4a) and March–April 2000 (Figure 4d) events do not have good RSL data coverage around the peak dates, but one can see that the switch to summer-like conditions has happened in the days following the peak date.

Another salient feature in these temperature plots is that the cooling of the upper mesosphere consistently precedes the peak date of the stratospheric wind reversal (Figures 4b, 4c, 4e, and 4f). In two cases, the cooling of the upper mesosphere even precedes the warming of the lower mesosphere (Figures 4b and 4e).

Table 1. List of Major SSWs and USU RSL Data

SSW Event	Peak Date	−40 Days	+40 Days	Nights of USU RSL Data
Jan–Feb 1995	05 Feb 1995	28 Dec 1994	17 Mar 1995	26
Dec 1998 to Jan 1999	17 Dec 1998	07 Nov 1998	26 Jan 1999	19
Feb–Mar 1999	07 Mar 1999	26 Jan 1999	16 Apr 1999	29
Mar–Apr 2000	21 Mar 2000	10 Feb 2000	30 Apr 2000	9
Jan–Mar 2001	17 Feb 2001	08 Jan 2001	29 Mar 2001	26
Jan–Feb 2003	18 Jan 2003	10 Dec 2002	27 Feb 2003	17

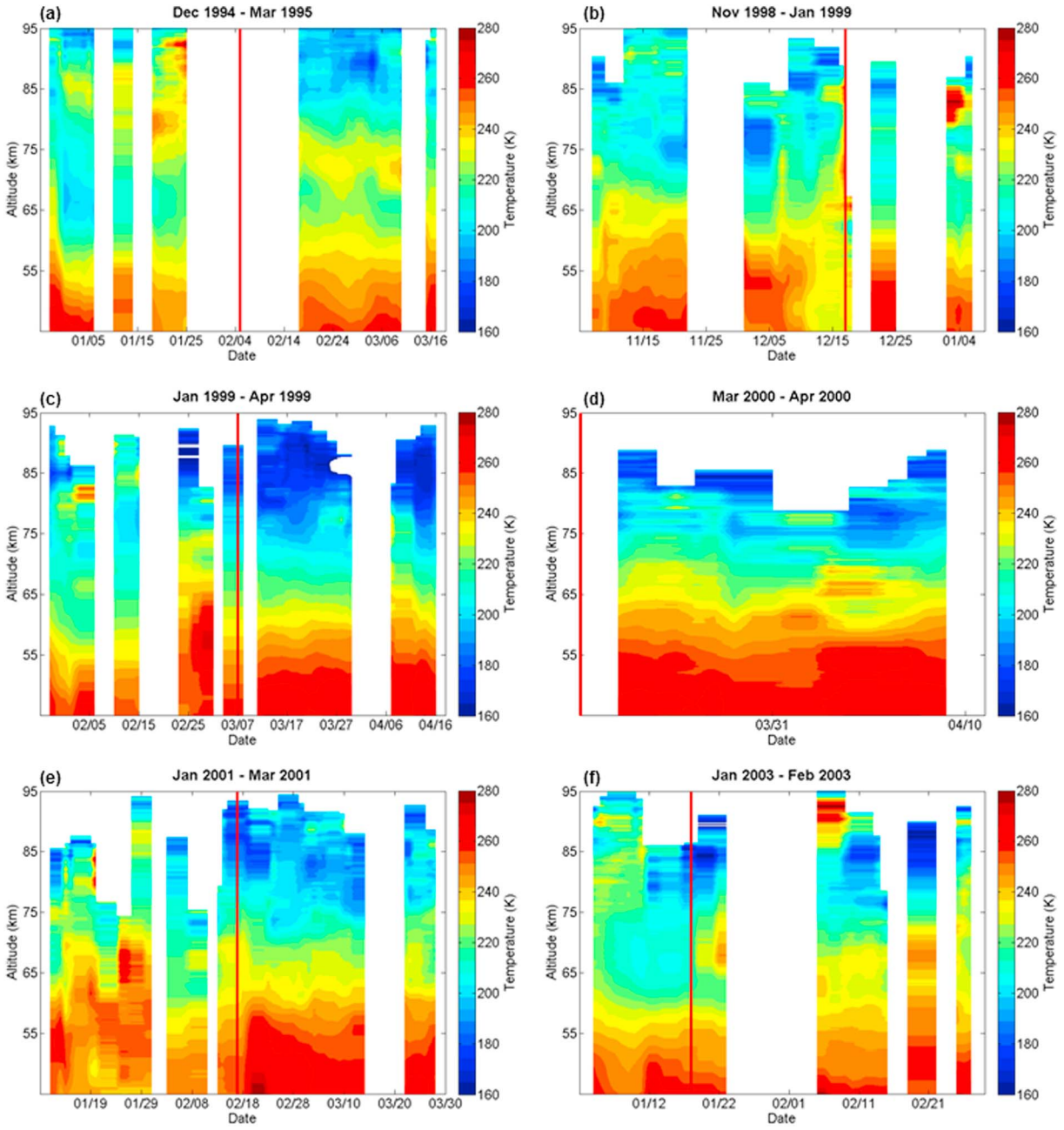

Figure 4. USU Rayleigh lidar nighttime temperatures for (a–f) six SSW event periods. Red vertical lines mark peak dates. Color bars are on the same scale as in Figure 2.

To better define the upper mesosphere coolings and lower mesosphere warmings, temperature difference plots (Figures 5a–5f) were created by subtracting the climatological 3 February profile from each nighttime temperature profile during each of the six SSW events. Because it was in the middle of the climatological period of interest (Figure 2a), 3 February was chosen. However, because the temperature climatology was averaged with at 31 day sliding window, the 3 February profile is really an average from 19 January to 18 February, which makes it more representative of winter climatological temperatures, overall. A climatological profile was chosen as opposed to a profile preceding the SSW or an average of winter nights' temperatures when there was no SSW, due to lack of data consistently acquired during these two periods.

In Figure 5, the dominant vertical pattern, which occurs near the peak date and continues for several weeks after, is made up of warmings in the upper stratosphere and lower mesosphere (45–65 km) and coolings in the upper mesosphere (65–90 km) (as seen in Figures 5b–5f). This pattern supports the switch in

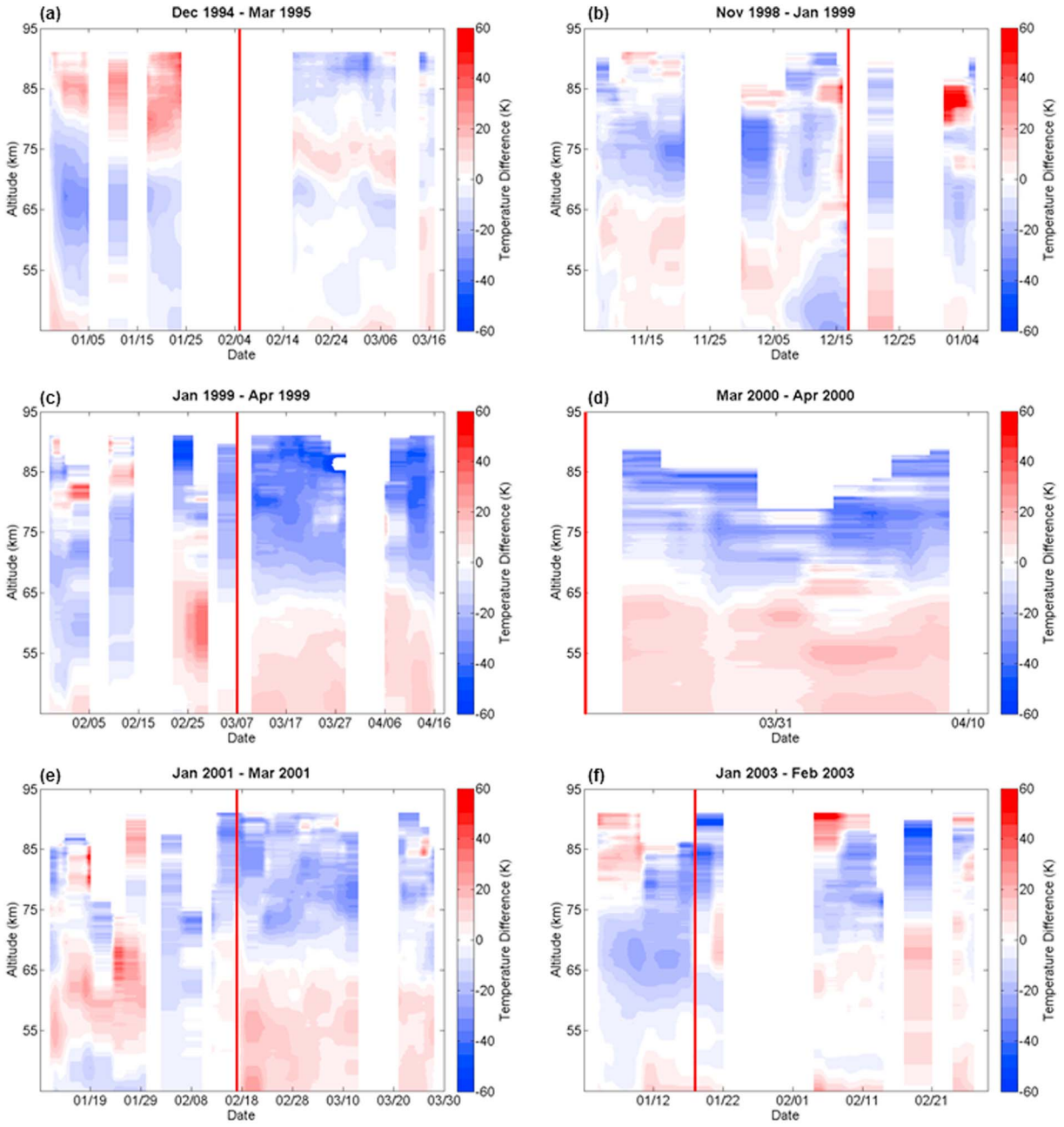

Figure 5. Temperature difference plots for the (a–f) six SSW event periods. Red vertical lines mark peak dates.

Figure 4 from winter-to-summer temperatures and assigns magnitudes to these mesospheric temperature anomalies. The coolings typically decrease by −30 or −40 K, and the warmings increase by +30 K. One extreme warming at the end of February 1999 attained a relative change of +40 K (Figure 5c) and corresponded to what appears to be an elevated stratopause event (elevated in both temperature and altitude). Unlike previously reported elevated stratopause events in the arctic [*Chandran et al.*, 2013], this event occurred prior to the peak of the SSW.

The uncertainty for the temperature differences (Figure 5), as a function of altitude and time, for each event, are given in Figure 6. The temperature difference uncertainties, $\sigma_{D_{ij}}$, are calculated as

$$\sigma_{D_{ij}} = \sqrt{\sigma_{T_{ij}}^2 + \overline{\sigma}_{C_i}^2}$$

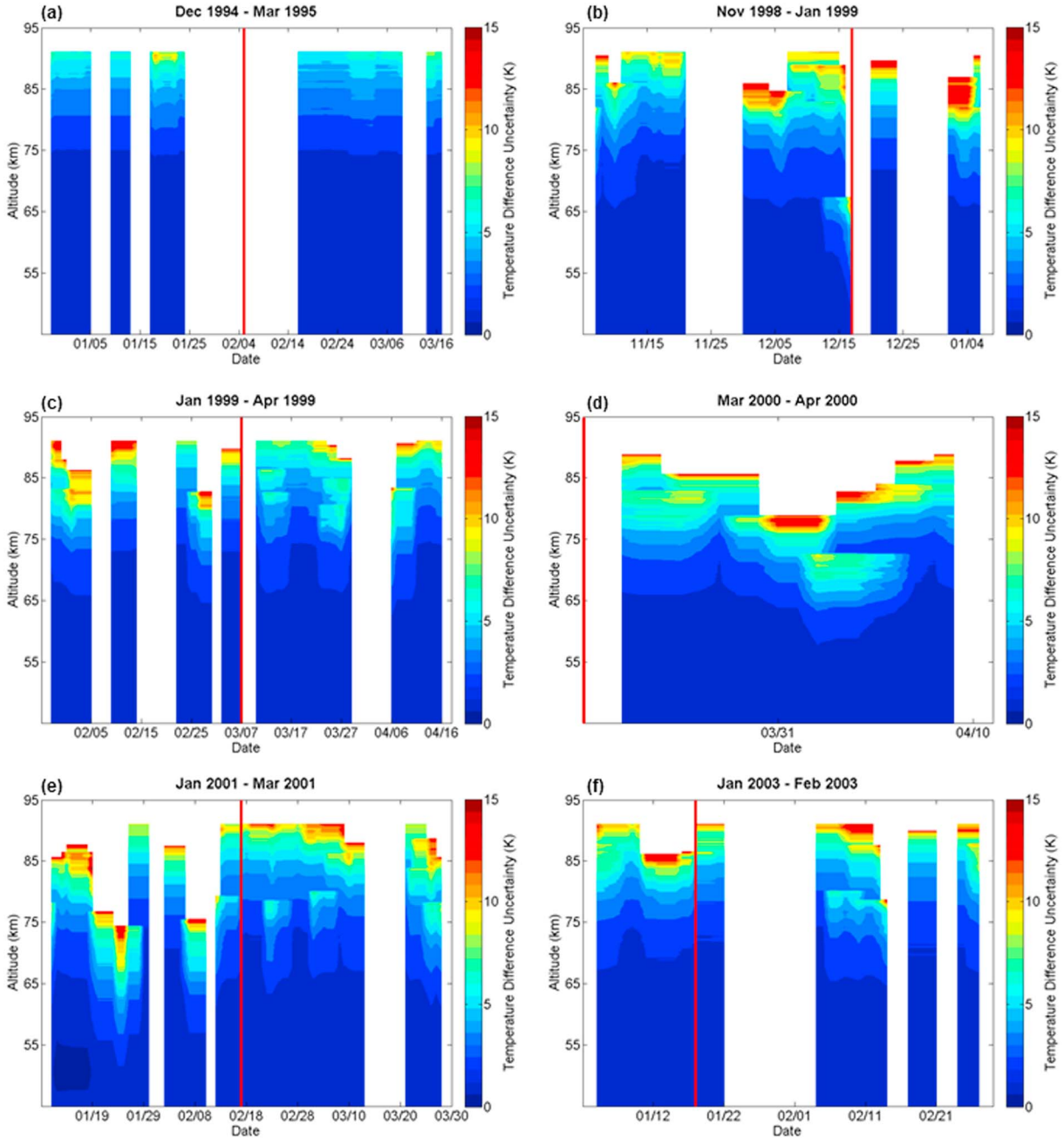

Figure 6. Temperature difference uncertainties for each of the six SSW event periods. Red vertical lines mark peak dates.

where $\sigma_{T_{ij}}$ is the standard deviation, based on Poisson statistics, of the temperatures for an individual night *j* at altitude *i* and $\overline{\sigma}_{C_i}$ is the RMS standard deviation of the mean of the temperature climatology (see error bars in Figure 3) for the 3 February climatological profile at altitude *i*.

It should be noted that these uncertainties are overestimated, because the variable smoothing from 1 to 5 days was not taken into account. For the most part, the uncertainty is between 1 and 10 K. This indicates that the consistent 20 to 40 K temperature differences shown in Figure 5 are statistically significant.

4. Discussion

The first midlatitude mesospheric temperature anomalies during a minor SSW event were shown with lidar observations made by *Hauchecorne and Chanin* [1983] at the Observatoire d'Haute Provence (OHP; 44°N, 6°E).

Their study showed a cooling of the low to middle mesosphere (50–70 km) of more than −20 K and a warming in the middle to upper stratosphere (30–45 km) also of about +20 K. Decades later, negative temperature anomalies in the tens of degrees at midlatitudes (54°N and 41°N) were observed higher into the mesosphere (80–90 km) [*Hoffmann et al.*, 2007; *Yuan et al.*, 2012]. Our observations agree in magnitude (maximum temperature anomaly of about −30 or −40 K at 80–90 km) with the anomalies presented in these case studies. They also manifest during all of the SSW periods in which there are overlapping USU RSL measurements. The observations presented in this paper suggest that these strong temperature changes at midlatitudes in the mesosphere are not limited to singular case studies, but rather occur consistently during most, if not all major SSW events.

While our observations from a single site do not capture the full longitudinal variability at midlatitudes during SSWs, our results do show a consistent mesospheric warming and cooling pattern during every observed event (in the 11 year observational period, there were eight major SSWs, and the USU RSL data set overlapped with all but two of these events). Furthermore, the magnitudes of these warmings and coolings are especially strong in magnitude, when compared with other midlatitude studies. Two model studies [*Chandran and Collins*, 2014; *Liu and Roble*, 2002] show zonal mean, SSW-induced temperature anomalies at roughly 42°N, which are significantly smaller in magnitude (up to ±10 K) than our temperature difference results (up to ±40 K). The RSL at OHP showed composite temperature anomalies for 13 SSW winters [*Angot et al.*, 2012], which gave significantly different results from what is presented in this paper. For the 20 days preceding the SSW event and about 10 days after, they showed coolings down to about −10 K in the upper mesosphere and warmings in the upper stratosphere and lower mesosphere up to about +15 K. These anomalies are again significantly smaller in magnitude than our results and also do not persist for as long after the peak day of the SSW. The discrepancy in magnitude between the USU RSL temperature anomalies and those presented in the aforementioned studies could be a signature of the longitudinal variability in the SSW event, itself. However, the fact that (a) temperature anomalies of about the same strength are shown during every observed SSW event, without much variation between the years, and (b) that the PW1 amplitudes in the upper stratosphere greatly decrease after the peak dates of all six SSW events (bottom panels in Figure 1) suggests that the magnitudes of the temperature anomalies seen at the USU RSL are not strictly a longitudinally based phenomena. To fully examine the longitudinal variability of these temperature anomalies, coordinated measurements among several individual sites spaced around the same latitude circle are needed.

Several studies have noted that observed anomalies in the mesosphere occur prior to the warming and wind reversal in the stratosphere [*Walterscheid et al.*, 2000; *Azeem et al.*, 2005; *Hoffmann et al.*, 2007; *Yuan et al.*, 2012]. While our observations do show the mesospheric coolings consistently precede the wind reversal peak, they do not always precede the warmings in the upper stratosphere/lower mesosphere (45–50 km) measured by our lidar. Figures 3b and 3e do show two cases of mesospheric coolings preceding both the wind reversal peak and the warming at lower altitudes. For two other cases, (Figures 3c and 3f), the mesospheric coolings happen prior to the peak wind reversal but do not precede the lower mesospheric warming. These results indicate that mesospheric coolings do not always precede stratospheric warmings at midlatitudes.

5. Conclusions

The midlatitude mesosphere's thermal structure during SSW events was studied using the USU RSL temperature data from 1993 to 2004. The RSL data set overlapped with six of the eight major SSWs that occurred during the 11 year period. Careful attention was paid in determining each of the SSW events in the polar stratosphere using NASA MERRA zonal mean temperatures and zonal winds both at the 10 hPa level and in defining the peak date of the wind reversal. From there, available USU RSL temperature profiles were presented for ±40 days around the peak date. These nighttime profiles were then compared with a wintertime climatological profile.

From this comparison, we saw that the thermal structure of the midlatitude mesosphere switches from winter (170–270 K) to summer (205–250 K) conditions in the span of only a few days around the peak date and persists for several days thereafter. Temperature deviations from the climatological 3 February profile showed that this switch resulted in warmings of the lower mesosphere up to +40 K and coolings in the upper mesosphere of down to −40 K. These magnitudes are consistent with the midlatitude case study results and are comparable with the temperature deviations typically seen in the polar mesosphere.

It has been noted in the past that mesospheric coolings have preceded stratospheric warmings. However, in the data presented here, this pattern was not seen throughout all of the events; only two of the six. However,

it is important to note that strong upper mesospheric coolings did exist during all of the observed SSW periods. In the past, case studies have suggested strong temperature changes at latitudes similar to the northern Utah USU RSL site. Our work clearly demonstrates a pattern of mesospheric connection that consistently extends down to the USU site at 42°N latitude during major SSW events.

Acknowledgments
MERRA data are available at http://acd-ext.gsfc.nasa.gov/Data_services/met/ann_data.html. USU RSL data are available from the authors upon request. The RSL data collection was supported by the National Science Foundation under grant ATM-9203034, ATM-9302118, ATM-9714789, and ATM-01234145. L.S. was supported through the Utah NASA Space Grant Consortium grant 120845 and by USU. Special thanks go to the dedicated student lidar operators.

References

Andrews, D. G., J. R. Holton, and C. B. Leovy (1987), *Middle Atmosphere Dynamics*, 489 pp., Academic Press, San Diego, Calif.
Angot, G., P. Keckhut, A. Hauchecorne, and C. Claud (2012), Contribution of stratospheric warmings to temperature trends in the middle atmosphere from the lidar series obtained at Haute-Provence Observatory (44°N), *J. Geophys. Res.*, *117*, D21102, doi:10.1029/2012JD017631.
Azeem, S. M. I., E. R. Talaat, G. G. Sivjee, H.-L. Liu, and R. G. Roble (2005), Observational study of the 4-day wave in the mesosphere preceding the sudden stratospheric warming events during 1995 and 2002, *Geophys. Res. Lett.*, *32*, L15804, doi:10.1029/2005GL023393.
Baldwin, M. P., and T. J. Dunkerton (2001), Stratospheric harbingers of anomalous weather regimes, *Science*, *294*, 581–584.
Beissner, K. C. (1997), Studies of mid-latitude mesospheric temperature variability and its relationship to gravity waves, tides, and planetary waves, PhD dissertation, 186 pp., Utah State Univ., Logan, Utah.
Chandran, A., and R. L. Collins (2014), Stratospheric sudden warming effects on winds and temperature in the middle atmosphere at middle and low altitudes: A study using WACCM, *Ann. Geophys.*, *32*, 859–874, doi:10.5194/angeo-32-859-2014.
Chandran, A., R. L. Collins, R. R. Garcia, D. R. Marsh, V. L. Harvey, J. Yue, and L. de la Torre (2013), A climatology of elevated stratopause events in the whole atmosphere community climate model, *J. Geophys. Res. Atmos.*, *118*, 1234–1246, doi:10.1002/jgrd.50123.
Charlton, A. J., and L. M. Polvani (2007), A new look at stratospheric sudden warmings. Part I: Climatology and modeling benchmarks, *J. Clim.*, *20*, 449–469, doi:10.1175/JCLI3996.1.
Chau, J. L., N. A. Aponte, E. Cabassa, M. P. Sulzer, L. P. Goncharenko, and S. A. González (2010), Quiet time ionospheric variability over Arecibo during sudden stratospheric warming events, *J. Geophys. Res.*, *115*, A00G06, doi:10.1029/2010JA015378.
de Wit, R. J., R. E. Hibbins, P. J. Espy, Y. J. Orsolini, V. Limpasuvan, and D. E. Kinnison (2014), Observations of gravity wave forcing of the mesopause region during the January 2013 major Sudden Stratospheric Warming, *Geophys. Res. Lett.*, *41*, 4745–4752, doi:10.1002/2014GL060501.
Goncharenko, L. P., J. L. Chau, H.-L. Liu, and A. J. Coster (2010), Unexpected connections between the stratosphere and ionosphere, *Geophys. Res. Lett.*, *37*, L10101, doi:10.1029/2010GL043125.
Hauchecorne, A., and M. L. Chanin (1980), Density and temperature profiles obtained by lidar between 35 and 70 km, *Geophys. Res. Lett.*, *7*, 565–568, doi:10.1029/GL007i008p00565.
Hauchecorne, A., and M. L. Chanin (1983), Mid-latitude lidar observations of planetary waves in the middle atmosphere during the winter of 1981–1982, *J. Geophys. Res.*, *88*(C6), 3843–3849, doi:10.1029/JC088iC06p03843.
Hedin, A. E. (1991), Extension of the MSIS thermosphere model into the middle and lower atmosphere, *J. Geophys. Res.*, *96*(A2), 1159–1172, doi:10.1029/90JA02125.
Herron, J. P. (2007), Rayleigh-scatter lidar observations at USU's atmospheric lidar observatory (Logan, UT)—Temperature climatology, temperature comparisons with MSIS, and noctilucent clouds, PhD dissertation, 156 pp., Utah State Univ., Logan, Utah.
Hoffmann, P., W. Singer, D. Keuer, W. K. Hocking, M. Kunze, and Y. Murayama (2007), Latitudinal and longitudinal variability of mesospheric winds and temperatures during stratospheric warming events, *J. Atmos. Sol. Terr. Phys.*, *69*, 2355–2366, doi:10.1016/j.jastp.2007.06.010.
Holton, J. R. (2004), *An Introduction to Dynamic Meteorology*, 535 pp., Academic Press, San Diego, Calif.
Labitzke, K. G. (1972), The interaction between stratosphere and mesosphere in winter, *J. Atmos. Sci.*, *29*, 1395–1399.
Labitzke, K. G., and H. van Loon (1999), *The Stratosphere: Phenomena, History and Relevance*, 189 pp., Springer, Berlin, Germany.
Laskar, F. I., and D. Pallamraju (2014), Does sudden stratospheric warming induce meridional circulation in the mesosphere thermosphere system?, *J. Geophys. Res. Space Physics*, *119*, 10,133–10,143, doi:10.1002/2014JA020086.
Limpasuvan, V., D. J. Thompson, and D. L. Hartmann (2004), The life cycle of the Northern Hemisphere sudden stratospheric warmings, *J. Clim.*, *17*, 2584–2596.
Liu, H.-L. and R. G. Roble (2002), A study of a self-generated stratospheric sudden warming and its mesospheric–lower thermospheric impacts using the coupled TIME-GCM/CCM3, *J. Geophys. Res.*, *107*(D23), 4695, doi:10.1029/2001JD001533.
Matsuno, T. (1971), A dynamical model of the stratospheric sudden warming, *J. Atmos. Sci.*, *28*, 1479–1494.
McIntyre, M. E., and T. N. Palmer (1983), Breaking planetary waves in the stratosphere, *Nature*, *305*, 593–600.
Quiroz, R. S. (1977), The tropospheric–stratospheric polar vortex breakdown of January 1977, *Geophys. Res. Lett.*, *4*, 151–154, doi:10.1029/GL004i004p00151.
Rienecker, M. M., et al. (2011), MERRA: NASA's modern-era retrospective analysis for research and applications, *J. Clim.*, *24*, 3624–3648.
Scherhag, R. (1952), Die explosionsartigen Stratosphärenäwärmungen des Spätwinters, *Ber. Dtsch. Wetterdienstes (US Zone)*, *6*, 51–63.
She, C. Y., S. Chen, Z. Hu, J. Sherman, J. D. Vance, V. Vasoli, M. A. White, J. R. Yu, and D. A. Krueger (2000), Eight-year climatology of nocturnal temperature and sodium density in the mesopause region (80 to 105 km) over Fort Collins, CO (41°N, 105°W), *Geophys. Res. Lett.*, *27*, 3289–3292, doi:10.1029/2000GL003825.
Siskind, D. E., L. Coy, and P. Espy (2005), Observations of stratospheric warmings and mesospheric coolings by the TIMED SABER instrument, *Geophys. Res. Lett.*, *32*, L09804, doi:10.1029/2005GL022399.
Thurairajah, B., S. M. Bailey, C. Y. Cullens, M. E. Hervig, and J. M. Russell III (2014), Gravity wave activity during recent stratospheric sudden warming events from SOFIE temperature measurements, *J. Geophys. Res. Atmos.*, *119*, 8091–8103, doi:10.1002/2014JD021763.
Walterscheid, R. L., G. G. Sivjee, and R. G. Roble (2000), Mesospheric and lower thermospheric manifestations of a stratospheric warming event over Eureka, Canada (80°N), *Geophys. Res. Lett.*, *27*, 2897–2900, doi:10.1029/2000GL003768.
Whiteway, J. A., and A. I. Carswell (1994), Rayleigh lidar observations of thermal structure and gravity wave activity in the high arctic during a stratospheric warming, *J. Atmos. Sci.*, *51*, 3122–3136.
Wickwar, V. B., T. D. Wilkerson, M. Hammond, and J. P. Herron (2001), Mesospheric temperature observations at the USU/CASS Atmospheric Lidar Observatory (ALO), *Proc SPIE*, *4153*, 272–284, doi:10.1117/12.417056.
Yamashita, C., H.-L. Liu, and X. Chu (2010), Responses of mesosphere and lower thermosphere temperatures to gravity wave forcing during stratospheric sudden warming, *Geophys. Res. Lett.*, *37*, L09803, doi:10.1029/2009GL042351.
Yuan, T., B. Thurairajah, C.-Y. She, A. Chandran, R. L. Collins, and D. A. Krueger (2012), Wind and temperature response of midlatitude mesopause region to the 2009 Sudden Stratospheric Warming, *J. Geophys. Res.*, *117*, D09114, doi:10.1029/2011JD017142.